High-Temperature Materials

SCIEPublish

Communication

Peculiarities of Radiation Synthesis of $MeWO_4$ Ceramics

Zhanar Bakiyeva [1], Victor Lisitsyn [2], Gulnur Alpysova [1], Anna Karnaukhova [2,*], Dossymkhan Mussakhanov [3], Dmitriy Afanasyev [1] and Mickhail Golkovski [4]

[1] Faculty of Physics and Engineering, Karaganda National Research University Named after E.A. Buketov, Karaganda 100024, Kazakhstan; Bakiyeva_Zh@karnu-buketov.edu.kz (Z.B.); Alpysova.G@karnu-buketov.edu.kz (G.A.); Afanasyev.D@karnu-buketov.edu.kz (D.A.)

[2] Department of Materials Science, National Research Tomsk Polytechnic University, 30, Lenin Ave., Tomsk 634050, Russia; lisitsyn@tpu.ru (V.L.)

[3] Faculty of Physics and Engineering, Eurasian National University Named after L.N. Gumilyov, Astana 010008, Kazakhstan; mussakhanov_da@enu.kz (D.M.)

[4] Budker Institute of Nuclear Physics, SB RAS, Novosibirsk 630090, Russia; m.g.golkovski@inp.nsk.su (M.G.)

* Corresponding author. E-mail: meleshko@tpu.ru (A.K.)

Received: 23 January 2026; Revised: 16 March 2026; Accepted: 10 April 2026; Available online: 30 April 2026

ABSTRACT: We report the results of $MeWO_4$ ceramics synthesis by the direct exposure of metal (Mg, Ca, Zn, W) oxides mixture to a high-power flux of high-energy electrons. The oxide powder particle sizes are 1–10 microns. The synthesis occurs with high efficiency in less than 1 s without the use of any additional substances and energy sources. The purpose of this work is to establish the main processes that ensure the effective synthesis of $MgWO_4$, $CaWO_4$, and $ZnWO_4$ ceramics from ZnO, CaO, MgO, and WO_4 oxides, which differ significantly in their physical and chemical properties. It has been found that the dependence of synthesis efficiency on the electron beam power density and the power density threshold at which synthesis begins varies significantly for simple metal oxides and is very close for the tungstates of these metals. The most probable explanation for the observed effect is redistribution of absorbed radiation energy. WO_3 powder particles have a high absorptance of the incident electron radiation. The result is a cascade multiplication of primary electrons into secondary electrons with much lower energy. Secondary electrons are efficiently absorbed by MgO, CaO, and ZnO particles, leading to their efficient decomposition and the formation of a new phase.

Keywords: Oxide ceramics; Tungsten; Radiation synthesis; Electron beam irradiation; Power density

1. Introduction

Metal tungstates, which are oxygen-containing tungsten compounds, are of considerable interest due to the variety and uniqueness of their properties. Tungstates of transition and alkaline earth metals with the general formula $MeWO_4$ (where Me = Ca, Mg, Pb, Cd, Zn, Co, Ni, *etc*.) are currently considered as one of the most promising groups of inorganic materials due to their outstanding physical and chemical properties [1,2]. Over the past decades, these materials have attracted researchers' attention due to their prospective applications in photocatalysis, optoelectronics, sensors, and energy.

Alkaline-earth tungstates ($CaWO_4$, $MgWO_4$) and transition metal tungstates ($ZnWO_4$, $CdWO_4$, $CoWO_4$, $NiWO_4$) are characterized by high transparency in the ultraviolet and visible ranges and are widely used as phosphors and scintillators in laser systems and radiation detectors. Due to their high scintillation characteristics, compounds of this class are also used in medical diagnostics, in particular in computed tomography [3,4]. An additional advantage of $MeWO_4$ based ceramic materials is their resistance to intense radiation, aggressive media, and high temperatures, which allows them to be used for detecting heavy charged particles, electrons, and X-rays [5].

Solid-phase synthesis remains the main method of the tungstate-based phosphors production. It is used for a variety of oxide and tungstate compounds [6–8]. This method is relatively simple and can produce materials in significant quantities, but requires high temperatures and long heat treatment. Other synthesis methods are also used, such as the coprecipitation method [9] and sol-gel technology [10]. However, all methods are characterized by multi-stage processes, the use of a large number of chemical reagents, the complexity of stoichiometry control, and the tendency to form mixed phases. As a result, the obtained materials often have a high concentration of both intrinsic and impurity defects, which lowers their optical and scintillation characteristics.

Radiation technologies for the synthesis of crystals and ceramics are becoming relevant [11]. Radiation synthesis is an express method with a number of key advantages [12]. Unlike traditional approaches, it allows to produce the ceramics from the charge, which components have significantly different melting points. The process occurs due to the energy of radiation only, without the additional reagents and the formation of extra phases. The short time of radiation synthesis (no more than 1 s) opens up prospects for creating and improving compounds with new properties. The nature of the processes that ensure high efficiency of radiation synthesis has been studied very little, although we have already managed to produce ceramics from about 20 refractory materials by now [12].

This work is aimed at establishing the main processes that ensure the synthesis of $MgWO_4$, $CaWO_4$, $ZnWO_4$ ceramics from ZnO, CaO, MgO, and WO_4 oxides, which differ significantly in their physical and chemical properties.

2. Materials and Methods

2.1. Methods of Radiation Synthesis of Ceramics

The synthesis of ceramics was carried out by direct exposure of an initial mixture of powders of a given composition to a high-energy electron beam [13]. The source of the required electron fluxes was the UNU Stand ELV-6 installation based on the ELV-8 accelerator, which generates electron fluxes with energies from 1.4 to 2.5 MeV and a power of up to 70 kW, developed and manufactured at the Budker Institute of Nuclear Physics of the Siberian Branch of the Russian Academy of Sciences, Novosibirsk. The electron beam was discharged into the open atmosphere through a differential pumping system. The beam had a Gaussian cross-section distribution, with the diameter on the irradiated surface about 1 cm. The initial mixtures of oxide powders in a stoichiometric ratio were loaded into copper crucibles with inner dimensions $5 \times 10 \times 0.7$ cm and mounted on a massive metal table to ensure efficient heat dissipation.

To synthesize the large-area samples, we used a dynamic scanning system: the electron beam moved across the surface of the crucible with a frequency of 50 Hz, while the crucible was shifted along at a constant speed of 1 cm/s. This irradiation mode ensured an even distribution of energy across the entire sample surface.

2.2. Materials for Radiation Synthesis of Ceramics

We used WO_3, ZnO, MgO, and CaO powders from Hebei Suoyi New Material Technology Co., Ltd. (Handan, China), with a purity of at least 99.95%, for the synthesis of $ZnWO_4$, $MgWO_4$, and $CaWO_4$

ceramics. The powders differ significantly in a number of physical characteristics, including melting point, crystalline and bulk density, which, in turn, affect the processes of radiation synthesis and the properties of the resulting ceramics. Table 1 presents the main parameters of the initial powders used in the research. The bulk density of the powder was calculated based on measurements of the powder mass in the crucible immediately before the electron irradiation. The powder was placed into the crucible and compacted. The volume of the powder was controlled to be constant. Table 1 also shows the values of the extrapolated path depth of electrons with energies of 1.4 MeV in these materials. Electron path depths, both in the charge and in the crystal, were calculated by the Monte Carlo method using modified Bethe's formula [14]. Details of the method and the calculation results are presented in Section 3.3.

Table 1. Characteristics of the initial materials for synthesis: ZnO, CaO, MgO, WO_3.

Initial Material	Crystalline Density, g/cm^3	Bulk Density, g/cm^3	Melting Temperature, °C	Electron Path Depth in the Charge, mm	Electron Path Depth in the Crystal, mm
ZnO	5.61 [15]	1.0	1974 [15]	5.48	1.15
CaO	3.34 [15]	1.2	2613 [15]	6.58	2.0
MgO	3.58 [15]	0.58	2825 [15]	11.9	2.0
WO_3	7.16 [16]	2.66	1473 [17]	2.05	0.77

The authors of [18] have shown that the efficiency of radiation synthesis depends heavily on the particle size of the powders. We have carried out an analysis of the initial powder dispersion by the laser diffraction method using a Shimadzu SALD-7101 laser particle size analyzer (Shimadzu Corporation, Tokyo, Japan). As can be seen from the results shown in Figure 1, all the studied powders have a wide range of particle sizes, and contain a greater number of small particles (less than 1 micron) than particles of a large fraction (>1 micron). However, the volume fraction of large particles significantly exceeds the contribution of small particles, so, as a result, the large particles mainly determine the characteristics and the effectiveness of radiation synthesis processes.

It should be emphasized that the particle distribution regions of different compounds overlap, which is important for the implementation of radiation synthesis. This overlap in the particle-size distributions of different powders leads to a more uniform distribution of electron-beam energy between them during radiation synthesis, providing similar reaction conditions across different components of the mixture and increasing the probability of homogeneous phase formation in the ceramic materials. As shown in [18], the synthesis efficiency may be reduced due to local non-stoichiometry when using powders with significant particle size differences. This fact confirms the relevance of controlling the granulometric composition of the precursors.

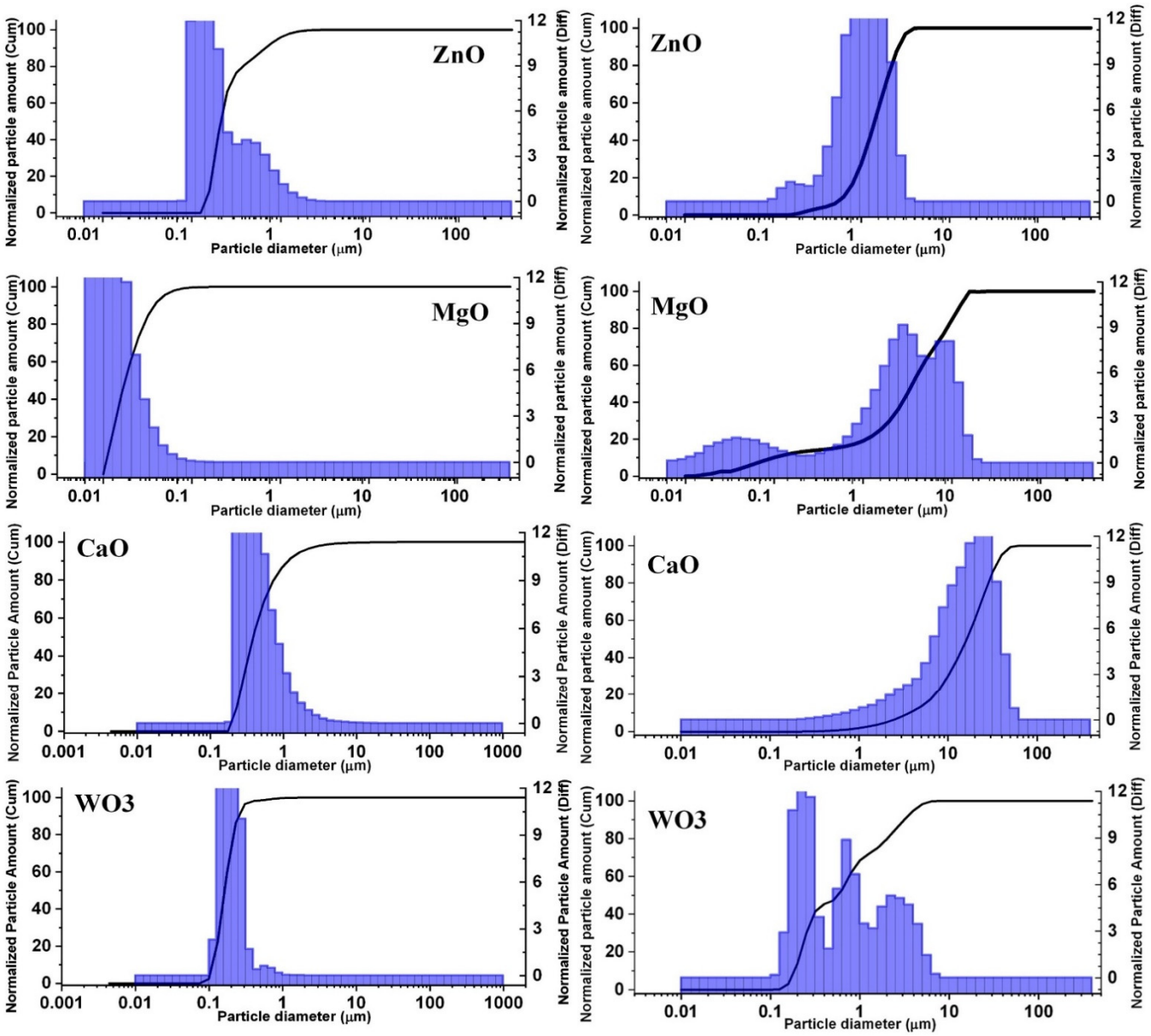

Figure 1. Distribution of the number (**on the left**) and volume (**on the right**) of the powder particles by their size.

3. Results and Discussion

3.1. Results of Ceramics Synthesis

We synthesized oxide ceramics from the above-described initial powders of MgO, CaO, ZnO, WO_3, and their mixtures ($MgWO_4$, $CaWO_4$, $ZnWO_4$, $Ca_{0.5}Mg_{0.5}WO_4$), which compositions are given in Table 2. A mixture of oxides in a stoichiometric ratio was placed in a stirrer cup. The stirring lasted for two hours. Table 2 also contains the parameters of electron irradiation in the "Scan" mode (electron energy E and flux power density P) and synthesis results (sample mass, density of the resulting porous ceramics, synthesis reaction yield). The yield of the synthesis reaction is understood here as the ratio of the sample mass to the charge mass. The beam power density was chosen for each of these powder mixtures, ensuring high process efficiency and ceramic quality. The synthesis of each ceramic sample was carried out at least 2 times. The difference in synthesis results is negligible.

Table 2. Irradiation modes, ceramics synthesis results.

Composition	E, MeV	P, kW/cm^2	Mass, g	Yield, %	Density, g/cm^3
MgO	1.4	25	20.13	95.7	2.3–2.4
CaO	1.4	26	42.80	74.80	– *
ZnO	1.4	20	44.00	92.90	3.0–3.1
WO_3	1.4	15	62.02	75.2	6.5
$MgWO_4$ (MgO–14.8%, WO_3–85.2%)	1.4	18	36.99	98.8	4.4–4.5
$CaWO_4$ (CaO–19.5%, WO_3–80.5%)	1.4	16	47.1	90.5	4.3–4.6
$Ca_{0.5}Mg_{0.5}WO_4$ (CaO–10%, MgO–7.2%, WO3–82%)	1.4	16	49.3	93.0	4.3–4.4
$ZnWO_4$ (ZnO–26%, WO_3–74%)	1.4	15	64.63	91.29	5.2

* The density of CaO ceramics is not given; it is difficult to measure it, since the produced samples are converted into $Ca(OH)_2$ powder in air.

Oxide ceramics MgO, ZnO, $MgWO_4$, $CaWO_4$, $Mg_{0.5}Ca_{0.5}WO_4$, $ZnWO_4$ are synthesized with a yield of at least 90%, and CaO and WO_3 ceramics—75%. The density of the ceramic samples is always much higher than that of the corresponding charge and is within the limits indicated in Table 2, but lower than the crystalline one (see Table 1), which is explained by the porosity of the samples.

Previously [13], we conducted an XRD analysis of $ZnWO_4$, $MgWO_4$, and $CaWO_4$ tungstates produced by the radiation synthesis method. The results show that the ceramics are formed mainly with the crystalline phases $ZnWO_4$, $MgWO_4$ (tetragonal), and $CaWO_4$. Also, additional phases were found in four samples in small quantities: WO_3 in the $CaWO_4$ sample, tungsten oxide W_3O_8, and triclinic magnesium tungsten oxide in $MgWO_4$.

Photos of the synthesized ceramics samples are shown in Figure 2.

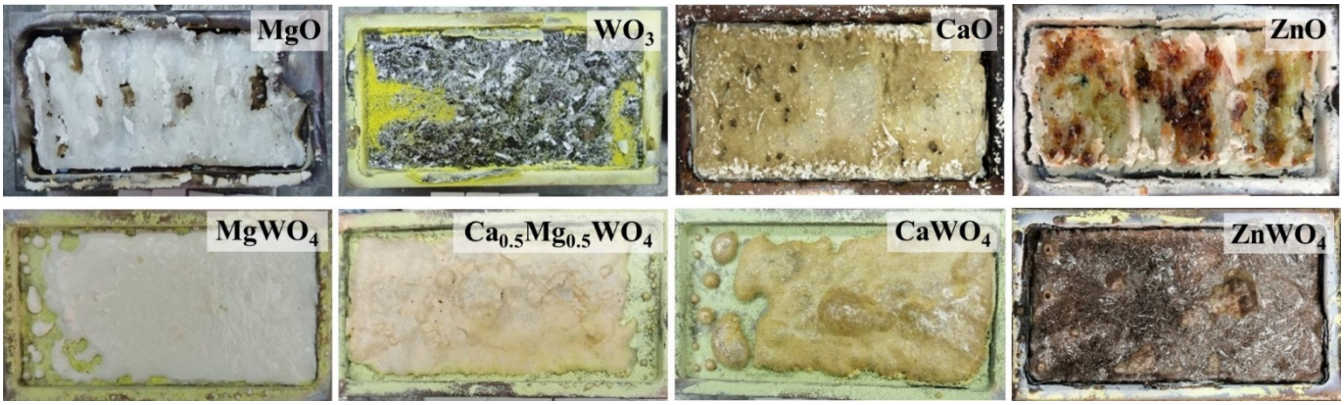

Figure 2. Photos of the synthesized ceramic samples in the crucibles with inner size 5 × 10 cm: upper row—simple oxides, lower row—complex tungsten-containing oxides.

The sizes of all the samples are close to the size of the crucible—about 10 × 5 cm^2, but the simple oxides have a more complex surface shape. They have "ridges" on a solid base. Transverse bands up to 1–2 cm wide with peaks in the center are clearly visible. The bands are formed when adjacent sections of the processed charge merge. "Grooves" or even empty zones may form between the bands. We emphasize that although the bands are formed along the direction of the beam scanning across the crucible, they are not the result of a single beam passage through an elementary section. During irradiation, the crucible was moved relative to the scanning beam at a speed of 1 cm/s. Thus, each band about 1 cm wide was formed in

about 100 passes of the scanning beam. The contraction into bands is similar to the effect observed for the liquid phase cooling. Ceramics made of MgO and CaO powders are transparent, ZnO has a characteristic brown hue, and WO_3 is dark brown in color. The obtained MgO and ZnO ceramics can be stored for a long time without change; CaO ceramics, however, actively interact with water in the air and are converted into $Ca(OH)_2$ hydroxide powder. Therefore, measuring the density of these ceramics is difficult. Unlike simple oxides, $MgWO_4$, $CaWO_4$, $ZnWO_4$, and $Mg_{0.5}Ca_{0.5}WO_4$ oxides form plates with a smooth surface under electron irradiation.

All samples of synthesized ceramics are porous. However, the thickness of the samples of MgO, ZnO, and CaO oxides is much larger (4–6 mm) than that of $MgWO_4$, $CaWO_4$, $Mg_{0.5}Ca_{0.5}WO_4$, and $ZnWO_4$ oxides (2 mm on average). It should be noted that the thickness of all complex oxide samples is almost the same and is close to the thickness of WO_3 oxide. This fact suggests that heavy tungsten ions play a dominant role in absorbing the energy of the electron flux.

3.2. Dependence of Synthesis Efficiency on the Electron Flux Power Density

We have carried out investigation of the dependence of the synthesis efficiency on the power density of the electron flux incident on the charge surface in the "No scan" mode, that is, in one pass of the electron beam along the crucible. The synthesis efficiency was estimated by the weight of the produced ceramics. The measurement results are shown in Figure 3.

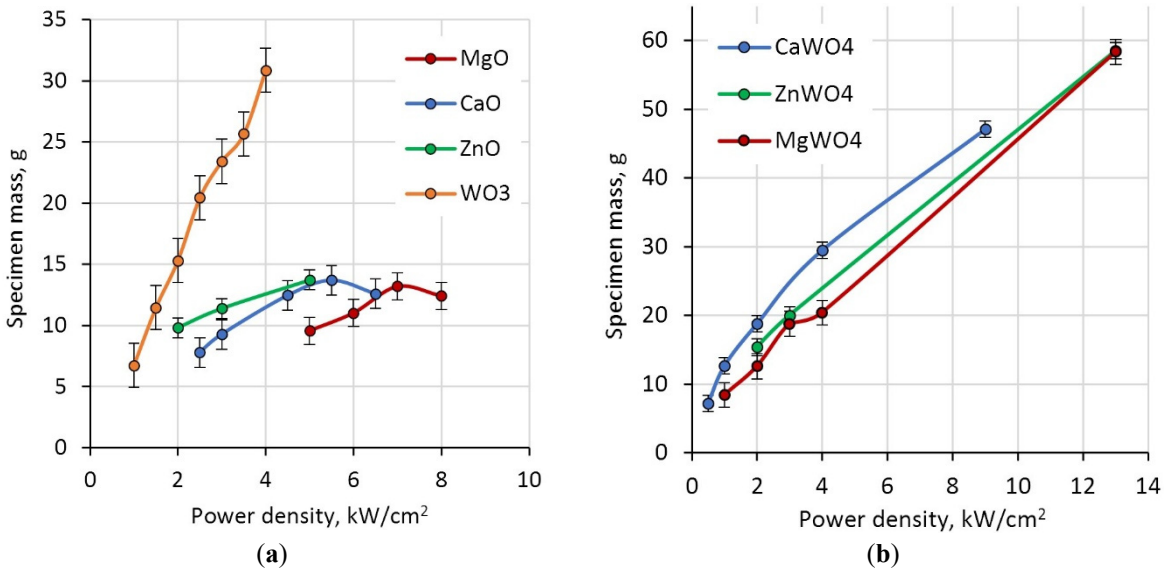

Figure 3. Dependence of the synthesized ceramics weight on the electron flux power density: (**a**) simple oxides; (**b**) complex oxides.

At the electron flux power density of 0.5 kW/cm^2, only a trace of darkened charge is observed on the surface of the charge for all used materials. As the power density increases, a narrow band of ceramics appears, and as the power density grows further, the band becomes denser, wider, and thicker. To measure the weight of the synthesized sample, we took it from the crucible and cleaned of the charge adhering to it. This procedure is easily implemented for big samples produced at high power density of radiation fluxes. However, small ceramic plates that appear in the charge at low power densities cannot be completely cleaned from the charge. That is why we do not put the starting points into the plots in Figure 3. Nevertheless, the dependence in Figure 3a indicates that the threshold for WO_3 ceramics synthesis is lower than for MgO, CaO, and ZnO. At high power densities, the weight of the sample increases due to an increase in the sample area [19]. We should note that the reasons for the observed special trend for WO_3 ceramics are currently unclear and will be the subject of further research.

As follows from the results shown in Figure 3b, the threshold values of the power density at which synthesis becomes possible are close for all studied metal tungstate ceramic samples ($ZnWO_4$, $MgWO_4$, $CaWO_4$) and amount to about 1 kW/cm^2. Pieces of ceramics are formed in the charge of all multicomponent mixtures, even at flux densities below 1 kW/cm^2, but the samples are too small to be taken into account. The dependence of the sample weight on the power density of the radiation flux is also quantitatively similar. Thus, complex oxide ceramics of all the studied compositions are formed with almost the same efficiency.

3.3. Calculation of Electron Energy Loss

From the above results on the similarity of synthesis thresholds for tungsten-containing oxides, the dependence of their synthesis efficiency on power density, the general similarity of the morphology of such samples, on the one hand, and the greater variety of these characteristics for simple oxides, on the other hand, it follows that tungsten plays a dominant role in the absorption of electron flux energy in the charge. We have performed a simulation of electron energy loss during passage through a substance by the Monte Carlo method using Win Casino v2.51 software [20]. The energy of the electron, suffering interaction from the scattering centers distributed randomly along its path, continuously loses its kinetic energy and can be calculated using Bethe's continuous slowing down approximation model [14]. A correction factor (Joy-Lod parameter) was introduced that allowed the formula to work correctly at low energies (below 1 keV).

Figure 4 shows the results of calculations of energy loss during the passage of electrons with 1.4 MeV energy through crystals and powders of the initial oxides. The extrapolated path depth of electrons with 1.4 MeV energy is 2.0 mm in MgO and CaO crystals, 1.15 and 0.77 mm in ZnO and WO_3 crystals, respectively. The electron path depth depends also on the bulk density, which in turn depends on the powder dispersion. The extrapolated path depth for 1.4 MeV electron in a charge of MgO, CaO, ZnO, and WO_3 powders is 11.9, 6.58, 5.48, and 2.05 mm, respectively. In the charge for $MgWO_4$, $CaWO_4$, and $ZnWO_4$ ceramics synthesis, the mass fraction of WO_3 is 85.2, 80.5, and 75%, respectively. Therefore, the electron path depth is determined mainly by the presence of tungsten oxide in the charge.

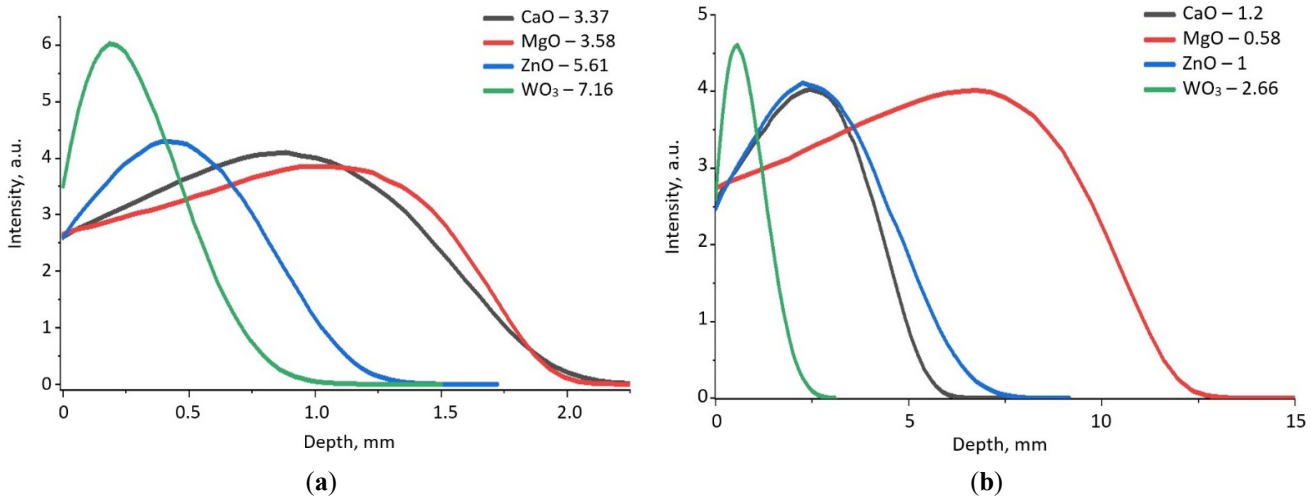

Figure 4. Extrapolated electron path depth in CaO, MgO, ZnO, and WO_3 oxides: (**a**) in crystals; (**b**) in charges with the bulk densities enlisted in Table 1. The bulk densities in g/cm^3 are indicated for each material.

The energy of primary electrons injected in dielectrics is transferred to the electrons of matter; electronic excitations appear and multiply in quantity, at the same time decreasing in energy. Multiplication continues until the energy of the secondary electrons is sufficient to transfer the electrons from the valence band to the conduction band. On average, it takes about $2E_g$ to create the final electronic excitations (that is, the energy of the electrons transfer from the middle of the valence band to the middle of the conduction

band). For example, when exposed to a 10 kW/cm^2 electron flux, the material absorbs about 5×10^{22} eV/cm^3 in 1 s. This energy is enough to create 10^{21} cm^{-3} electronic excitations, which exceeds the number of unit cells ($1–3 \times 10^{20}$ cm^{-3}) [21,22].

In our case, the flux of primary electrons transfers its energy mainly to the ions contained in the WO_3 powder particles. A cascade process of secondary electron generation occurs [19,23]. All the surrounding simple oxide particles end up in the field of electrons with much lower energies and absorb them effectively. Therefore, the volumetric density of the energy loss is much higher in the vicinity of a WO_3 powder particle than in a homogeneous charge of MgO, CaO, and ZnO. Such a significant increase in the volumetric loss of the local energy may be sufficient to initiate radiation-stimulated processes of element exchange between particles of the initial mixture with the formation of $MgWO_4$, $CaWO_4$, and $ZnWO_4$ ceramics.

4. Conclusions

The radiation method of refractory ceramics synthesis makes it possible to produce efficiently $MgWO_4$, $CaWO_4$, and $ZnWO_4$ ceramics from ZnO, CaO, MgO, and WO_4 oxides, which differ significantly in their physical and chemical properties.

The data on the dependence of the ceramic synthesis efficiency on the power density of the electron flux incident on the surface of the charge, as well as the results of the calculation of the extrapolated electron path in the studied oxides, show that tungsten plays a dominant role in the absorption of the electron flux energy by the charge.

We assume the following mechanism of radiation energy absorption. The flux of primary electrons transfers its energy mainly to the ions contained in WO_3 powder particles. There is a cascade process of secondary electron generation with much lower energy, which is effectively absorbed by all surrounding oxide particles. Such a significant increase in volumetric local loss of energy may be enough to initiate radiation-stimulated processes of element exchange between the initial materials particles with the formation of $MgWO_4$, $CaWO_4$, and $ZnWO_4$ ceramics.

Statement of the Use of Generative AI and AI-Assisted Technologies in the Writing Process

AI tools were used for language translation (with the authors taking full responsibility for the final content).

Acknowledgments

The authors are grateful to E.F. Polisadova of Tomsk Polytechnic University for her assistance in organizing measurements of the granulometric composition of precursors.

Author Contributions

Conceptualization, V.L.; Methodology, G.A. and Z.B.; Validation, V.L. and A.K.; Formal Analysis, D.M. and D.A.; Investigation, Z.B.; Resources, M.G.; Data Curation, A.K.; Writing—Original Draft Preparation, Z.B. and V.L.; Writing—Review & Editing, A.K.; Visualization, Z.B. and A.K.; Supervision, V.L.; Project Administration, V.L.; Funding Acquisition, V.L.

Ethics Statement

Not applicable.

Informed Consent Statement

Not applicable.

Data Availability Statement

Data will be available on request.

Funding

This research was funded by the Russian Science Foundation, grant number 23-73-00108. https://rscf.ru/project/23-73-00108/ (accessed on 23 January 2026).

Declaration of Competing Interest

The authors declare that they have no known competing financial interests or personal relationships that could have appeared to influence the work reported in this paper.

References

1. Hoang K, Oh M, Choi Y. Electronic structure, polaron formation, and functional properties in transition-metal tungstates. *J. RSC Adv.* **2018**, *8*, 4191–4196. DOI:10.1039/c7ra13436c
2. Skjærvø SL, Anker AS, Wied MC, Kjær ET, Juelsholt M, Christiansen TL, et al. Atomic structural changes in the formation of transition metal tungstates: The role of polyoxometalate structures in material crystallization. *Chem. Sci.* **2023**, *14*, 4806–4816. DOI:10.1039/d3sc00426k
3. Jeong HY, Lim HS, Lee JH, Heo J, Kim HN, Cho SO. $ZnWO_4$ nanoparticle scintillators for high resolution X-ray imaging. *Nanomaterials* **2020**, *10*, 1721–1729. DOI:10.3390/nano10091721
4. Min S, Choi S, Pajovic S, Vaidya S, Rivera N, Fan S, et al. End-to-end design of multicolor scintillators for enhanced energy resolution in X-ray imaging. *Light Sci. Appl.* **2025**, *14*, 158. DOI:10.48550/arXiv.2410.08543
5. Pudza I, Pudzs K, Tokmakovs A, Strautnieks NR, Kalinko A, Kuzmin A. Nanocrystalline $CaWO_4$ and $ZnWO_4$ tungstates for hybrid organic–inorganic X-ray detectors. *Materials* **2023**, *16*, 667. DOI:10.3390/ma16020667
6. Dabkowska HA, Dabkowski AB, Hermann R, Priede J, Gerbeth G. 8—Floating zone growth of oxides and metallic alloys. In *Handbook of Crystal Growth: Bulk Crystal Growth*, 2nd ed.; Rudolph P, Ed.; Elsevier: Amsterdam, The Netherlands, 2015; Volume 2A, pp. 281–329. DOI:10.1016/B978-0-444-63303-3.00008-0
7. Miller W, Sabanskis A, Gybin A, Gradwohl K, Wintzer A, Dadzis K, et al. A coupled approach to compute the dislocation density development during Czochralski growth and its application to the growth of high-purity germanium (HPGe). *Crystals* **2023**, *13*, 1440–1457. DOI:10.3390/cryst13101440
8. Patnaik M, Yadav P, Rout E, Yadav AK, Jha SN, Tyagi M, et al. A comprehensive study on the structural, radioluminescence and thermoluminescence properties of scheelite and wolframite type tungstates. *Rad. Phys. Chem.* **2024**, *223*, 111957. DOI:10.1016/j.radphyschem.2024.111957
9. Azadmehr S, Tafreshi MJ, Alamdari S. Synthesis, characterization and scintillation response of $ZnWO_4$-GO nanocomposite. *J. Compos. Compd.* **2022**, *4*, 158–162. DOI:10.52547/jcc.4.3.5
10. Garibay-Alvarado JA, Reyes-López SY. Sol-gel ceramics for SEIRAS and SERS substrates. *Crystals* **2021**, *11*, 439. DOI:10.3390/cryst11040439
11. Lisitsyn V, Tulegenova A, Kaneva E, Mussakhanov D, Gritsenko B. Express synthesis of YAG:Ce ceramics in the high-energy electrons flow field. *Materials* **2023**, *16*, 1057. DOI:10.3390/ma16031057
12. Lisitsyn V, Tulegenova A, Golkovski M, Polisadova E, Lisitsyna L, Mussakhanov D, et al. Radiation synthesis of high-temperature wide-bandgap ceramics. *Micromachines* **2023**, *14*, 2193. DOI:10.3390/mi14122193
13. Alpyssova G, Lisitsyn V, Bakiyeva Z, Chakin I, Kaneva E, Afanasyev D, et. al. Characterization of $ZnWO_4$, $MgWO_4$, and $CaWO_4$ ceramics synthesized in the field of a powerful radiation flux. *Ceramics* **2024**, *7*, 1085–1099. DOI:10.3390/ceramics7030071
14. Joy DC, Luo S. An empirical stopping power expression for low energy electrons. *Scanning* **1989**, *11*, 176–180. DOI:10.1002/sca.4950110404
15. Haynes WM. *CRC Handbook of Chemistry and Physics*, 97th ed.; CRC Press: Boca Raton, FL, USA, 2016; pp. 4-54–4-95.
16. Vemuri RS, Engelhard MH, Ramana CV. Correlation between surface chemistry, density, and band gap in nanocrystalline WO_3 thin films. *ACS Appl. Mater. Interfaces* **2012**, *4*, 1371−1377. DOI:10.1021/am2016409
17. Schneider SJ. *Compilation of the Melting Points of the Metal Oxides*; National Bureau of Standards: Washington, DC, USA, 1963; pp. 28–29.

18. Lisitsyn VM, Karipbayev ZT, Zhilgildinov ZS, Zhunusbekov AM, Tulegenova AT, Golkovski MG. Effect of precursor prehistory on the efficiency of radiation-assisted synthesis and luminescence of YAG: Ce ceramics. *Photonics* **2023**, *10*, 494. DOI:10.3390/photonics10050494
19. Chaynikov AP, Kochur AG, Dudenko AI. Cascade energy reemission by the silver atom ionized by 0.01–100 keV photons. Possible application of silver-based radiosensitizing agents in photon beam radiation therapy. *J. Electron Spectrosc. Relat. Phenom.* **2024**, *275*, 147472. DOI:10.1016/j.elspec.2024.147472
20. Drouin D, Couture AR, Joly D, Tastet X, Aimez V, Gauvin R. CASINO V2.4: A fast and easy-to-use modeling tool for scanning electron microscopy and microanalysis users. *Scanning* **2007**, *29*, 92–101. DOI:10.1002/sca.20000
21. Lisitsyn VM, Korepanov VI, Yakovlev VY. Evolution of primary radiation defectiveness in ionic crystals. *Russ. Phys. J.* **1996**, *39*, 5–29. DOI: 10.1007/BF02436146
22. Lushchik C, Feldbach E, Frorip A, Kirm M, Lushchik A, Maaroos A, et al. Multiplication of electronic excitations in CaO and $YAlO_3$ crystals with free and self-trapped excitons. *J. Phys. Condens. Matter* **1994**, *6*, 11177. DOI: 10.1088/0953-8984/6/50/025
23. Kochur AG, Chaynikov AP, Dudenko AI, Levitskaya VP. Final ion formation and energy reemission upon a cascade decay of single vacancies in the K and L electron shells of atomic platinum. *Bull. Karaganda Univ. Phys. Ser.* **2024**, *4*, 60–67. DOI:10.31489/2024ph4/60-67